Chemical Engineering Journal 99 (2004) 237–245

Chemical Engineering Journal

www.elsevier.com/locate/cej

Intrinsic kinetics of first-order reactions in photocatalytic membranes and layers

Richard K. Herz*

Chemical Engineering Program, Department of Mechanical and Aerospace Engineering, University of California, San Diego, CA 92093-0411, USA

Received 21 June 2003; accepted 15 November 2003

Abstract

Heterogeneous photocatalysts, in the form of particles immobilized in permeable membranes or in layers covering supports, are under development for production of ultrapure water for use in semiconductor fabrication and other applications. Concentration and light intensity gradients present within a photocatalyst layer will cause local reaction rates to vary within the layer, complicating determination of intrinsic kinetics. Analytical solutions are obtained here for arbitrary networks of two or more species that undergo first-order reactions in photocatalyst layers. First-order or pseudo-first-order behavior should be obtained at the very low contaminant concentrations encountered in water ultrapurification. Experimental data can be analyzed using the solutions to obtain estimates of intrinsic rate coefficients for two flow configurations: (1) water and reactants flow through a photocatalyst layer, (2) water flows past one face of a photocatalyst layer into which reactants diffuse, with the other face sealed. A set of experimental data in the literature is analyzed and an estimate of the intrinsic reaction rate coefficient is obtained. The analytical solutions show that, when reactants flow through a photocatalyst layer, the same outlet composition is obtained for the same total incident light intensity, regardless of how the incident intensity is distributed between the two faces of the layer. When reactants diffuse into a photocatalyst layer, greater conversion can be obtained for light incident on the face over which water flows than for light incident on the sealed face. Greater conversion is obtained for reactant flow through a photocatalyst layer than for reactant diffusion into the layer.

Keywords: Kinetics; Network; Photocatalyst; Reaction; Reactor; Water purification

1. Introduction

Heterogeneous photocatalysts are solid semiconductors that absorb light to produce energetic electron–hole pairs that participate in catalyzing reactions at the solid surface. Ions or radicals produced may initiate other reactions in the surrounding vapor or liquid [1]. A variety of materials have been studied, including TiO_2, CdS, MoO_2, $NaTaO_3$ and sensitized organic polymers. Reactions catalyzed include water dissociation to H_2 and O_2, NO and CO_2 reduction, and oxidation of organics [1–4]. A major application is destruction of organic pollutants in air and water by TiO_2-based catalysts [4–6]. In most studies of water purification, aqueous suspensions of the solid catalyst particles are used and hydrogen peroxide and ozone may be added as oxygen sources [7]. Photocatalysts immobilized as a layer over a solid surface or within a porous or permeable support layer have the advantage of automatic separation of catalyst and water [7–10]. Use of immobilized photocatalyst layers is imperative in the removal of trace contaminants by heterogeneous photocatalysis to produce ultrapure water for the semiconductor fabrication industry [11].

The rates of reactions carried out in a photocatalyst layer will vary with position within the layer because of light intensity gradients caused by light absorption and because of concentration gradients caused by conversion or diffusion resistance. Unless these gradients are taken into account, rate coefficient values determined will be averages that have limited use. The purpose of this work is to provide models that take these gradients into account and that can be used for design and for determination of intrinsic rate coefficient values.

The photocatalytic oxidation of organic molecules can occur through a sequential pathway involving the production of one or more intermediate species [12–14]. At relatively high concentrations, rates on heterogeneous photocatalysts may have a Langmuir–Hinshelwood dependence on concentration with an apparent adsorption constant in the denominator of the rate expression [14,15]. Langmuir–Hinshelwood

* Tel.: +1-858-534-6540; fax: +1-858-534-4543.
E-mail address: herz@reactorlab.net (R.K. Herz).

1385-8947/$ – see front matter © 2003 Elsevier B.V. All rights reserved.
doi:10.1016/j.cej.2003.11.013

Nomenclature

A	geometric area of face of photocatalytic layer (m^2)
c	concentration ($mol\,m^{-3}$)
D_{eff}	effective diffusivity ($m^2\,s^{-1}$)
f	arguments of Bessel functions (dimensionless)
I_0	incident light intensity (lx)
$I_{0/1}$	modified (hyperbolic) Bessel functions
k	reaction rate coefficient ($lx^{-1}\,s^{-1}$)
$k' = kI_0$	reaction rate coefficient (s^{-1})
$\mathbf{K}$	rate coefficient matrix (dimensionless)
$K_{0/1}$	modified (hyperbolic) Bessel functions
l	distance into photocatalytic layer (m)
L	thickness of photocatalytic layer (m)
m	number of measurements
n	number of species
Q	flow rate through photocatalytic reaction cell ($m^3\,s^{-1}$)
r	reaction rate per unit volume catalyst ($mol\,s^{-1}\,m^{-3}$)
V	volume of fluid in system (m^3)
x	dimensionless position in layer $= l/L$
$\mathbf{X}$	eigenvector matrix (dimensionless)
y	real-species mole fraction
$\mathbf{Y}$	matrix of experimental mole-fraction measurements
z	eigenspecies concentration (dimensionless)

Greek letters

α	dimensionless light absorption coefficient $= \alpha' L$
α'	light absorption coefficient for specific photocatalyst (m^{-1})
γ	fraction of total light intensity incident on inlet face in case 1
δ	fractional conversion across reaction cell
η_i	effectiveness factor in diffusion cases 2 and 3 (dimensionless)
λ_i	eigenvalue in convection case 1 (dimensionless)
λ_i^2	eigenvalue in diffusion cases 2 and 3 (dimensionless)
$\mathbf{\Lambda}$	eigenvalue matrix in convection case 1 (diagonal, dimensionless)
τ	superficial residence time of fluid flowing through layer $= AL/Q$ (s)
$[\phi^2]$	non-diagonal matrix of ϕ_i^2 (dimensionless)
$[\lambda^2]$	eigenvalue matrix in diffusion cases 2 and 3 (diagonal, dimensionless)
ϕ_i^2	dimensionless rate coefficient in diffusion cases 2 and 3
ω_i	ratio of $z_i(x)$ to inlet value of z_i (case 1); ratio of inlet value of z_i to z_i inside reactor over external face of photocatalyst (case 2)
$\mathbf{\Omega}$	diagonal matrix of ω_i (dimensionless)

kinetics approach first-order kinetics at low concentrations [16], such as levels present in water ultrapurification. For example, the apparent adsorption constants reported by Rivas et al. [13] for a series of *n*-alkanoic acids, show that reaction rates for these acids approach first-order behavior at concentrations below 10 ppm.

Fig. 1 is a schematic of a system that could be used for ultrapurification of water. In the top half of Fig. 1, water is pumped from a well-mixed reservoir through a porous photocatalytic membrane and then is returned to the reservoir. The bottom half of the figure shows alternative configurations discussed below. The points in Fig. 2 are concentrations of species in the reservoir during a computer-simulated experiment. Input rate coefficient values are listed in Table 1. The physical dimensions and time scale of the computer simulation are characteristic of laboratory studies reported in the literature. Reactant A is sequentially converted to intermediate B, which is then converted to final product C, which may represent carbon dioxide and water. Con-

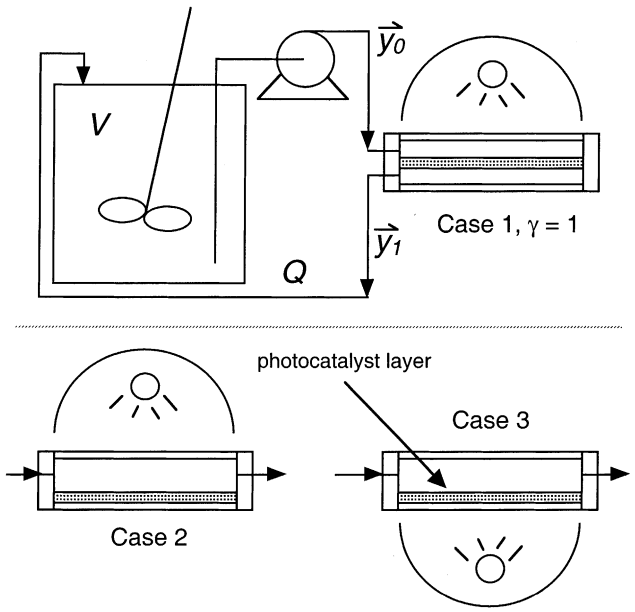

Fig. 1. Top: schematic diagram of system for ultrapurification of water with water flowing through a photocatalytic membrane and light incident on the inlet face of the membrane (case 1, $\gamma = 1$). A cross-section of the disk-shaped reaction cell is shown on the right, with the cylindrical axis of the cell oriented vertically. The reaction cell consists of, from top to bottom, a transparent window, the inlet water space, photocatalytic membrane (shaded), the outlet water space, and the bottom enclosure of the cell. Bottom: water flow and photocatalyst configurations for cases 2 and 3 in which water flows over the external face of the photocatalyst layer and reactants diffuse into the layer. In case 3, the bottom enclosure of the cell is a transparent window.

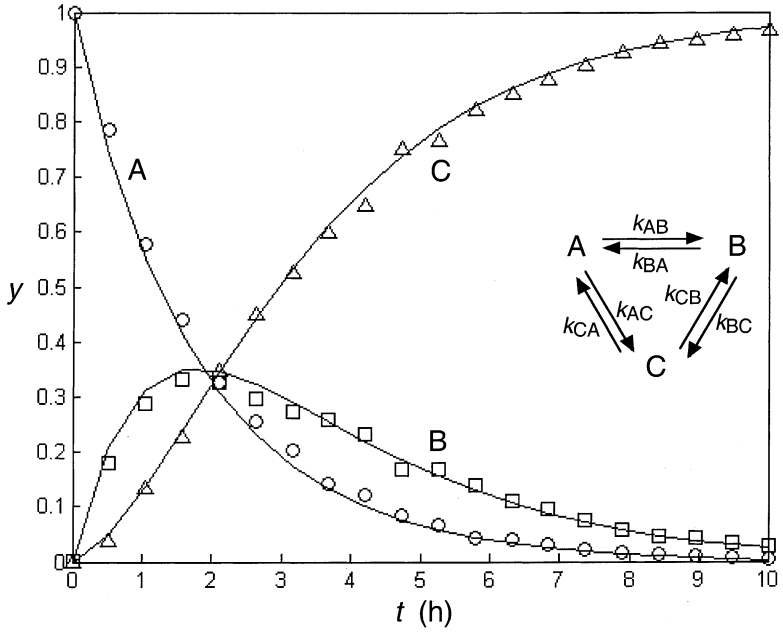

Fig. 2. Three-species example. Points: mole fraction data points y_i obtained in a computer-simulated experiment in the system of Fig. 1, case 1. Points were computed by numerical integration of Eqs. (3)–(5) using the input k' in Table 1, $A = 5.0 \times 10^{-3}\,\mathrm{m}^2$, $L = 5.0 \times 10^{-5}\,\mathrm{m}$, $Q = 1 \times 10^{-6}\,\mathrm{m}^3/\mathrm{s}$, $V = 1 \times 10^{-3}\,\mathrm{m}^3$, $\alpha = 1$, $\gamma = 1$, with random error added to the y_A and y_B (normal distribution with standard deviation = 5% of reading), and y_C obtained such that $\Sigma y_i = 1$. Lines: predictions computed using the estimated k' in Table 1, which were obtained by analyzing the mole fraction data points.

centrations of any added oxygen or ozone would be held constant.

Fig. 3 shows the light intensity and mole fraction variations across the photocatalyst layer at the start of the run, computed using the solutions obtained below. Because of the variation in reactant concentration and light intensity in the photocatalyst layer, the local rate varies with position. An analysis which ignores these gradients in the catalyst will underestimate rate coefficient values. Chen et al. [17] performed experiments which demonstrate the influence of external and internal transport resistances over photocatalyst layers.

The method of analysis described here allows determination of intrinsic rate coefficients for an arbitrary network of two or more species which undergo reactions with first-order or pseudo-first-order kinetics. Each pair of species in the network may be connected by reactions.

Numerical integration of coupled differential equations can be used to solve reaction networks, whether linear or nonlinear. An alternate solution strategy is used here to solve linear networks. The strategy is to apply a transformation to the system such that species in the transformed system are uncoupled and react independently. With such a simplified system, analytical solutions may be obtained for the transformed species. Then the reverse-transformation can be applied to get the concen-

Table 1
Reaction rate coefficients, $k'\,(\mathrm{s}^{-1}) = kI_0$

Inputs to Fig. 2 points, components of **K**	Estimates from analysis, components of $\mathbf{K}_{expl}$
$k'_{AB} = 1.0$	$k'_{AB} = 1.1$
$k'_{BC} = 1.0$	$k'_{BC} = 1.0$
$k'_{BA} = 0.00$	$k'_{BA} = 0.05$
$k'_{CB} = 0.00$	$k'_{CB} = 0.06$
$k'_{AC} = 0.00$	$k'_{AC} = 0.01$
$k'_{CA} = 0.00$	$k'_{CA} = 0.04$

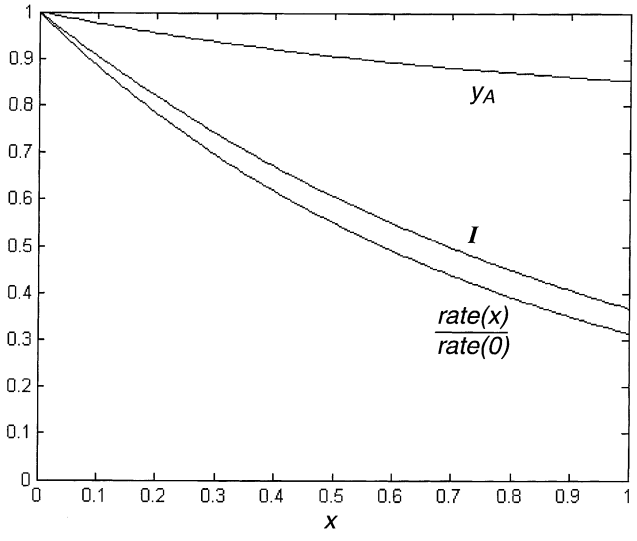

Fig. 3. Variation of mole fraction of species A, y_A, light intensity, I, and relative reaction rate within the photocatalytic layer of Fig. 1 at the start of the computer-simulated experiment shown in Fig. 2. This figure demonstrates the importance of taking light and concentration gradients into account when analyzing data to obtain intrinsic rate coefficients.

trations of the real species. This strategy was introduced into chemical kinetics by Wei and Prater [18], who also discussed conditions under which surface-catalyzed reactions can be modeled with pseudo-first-order kinetics. Wei [19] discussed application of the approach to reaction in heterogeneous, non-photocatalytic catalysts with diffusion resistance. Clement [20] applied the strategy to models of groundwater contaminant plumes. The method can also be used to estimate values of unknown rate coefficients from experimental measurements, as shown by Wei and Prater [18]. Gavalas [21] and Herz and Hegedus [22] showed how to do this with efficient experimental procedures.

Three cases are considered. In each, the photocatalyst is a permeable plane slab with light and concentration gradients in the direction normal to the face of the slab, e.g., a disk with a sealed circumference, or a film coating a surface.

2. Case 1—water flows through layer

For a layer that is illuminated on the face through which water enters, the rate of formation of species i in reaction j at dimensionless position x is:

$$r_{ij} = k_{ij} I_0 \, \mathrm{e}^{-\alpha x} c_i \tag{1}$$

where $0 \le x \le 1$, k_{ij} is the rate coefficient, α is the dimensionless light absorption coefficient, and c_i is the concentration of species i. This rate, which is per unit volume of catalyst layer, can also be expressed per unit mass of catalyst by dividing by catalyst layer density. The solution below remains valid when an additional intensity exponent, as used by Ollis [23], modifies the illumination intensity I_0 and the exponential term. Rivas et al. [13] concluded there was negligible effect of variation in illumination wavelength in their photocatalytic membranes. In cases 1–3 below, I_0 is the illumination intensity at the photocatalyst layer surface, after correction for light absorption by reactor windows and water outside the layer.

When the illumination intensity is distributed between the inlet and outlet faces, with γ equal to the fraction incident on the inlet face, the rate is:

$$r_{ij} = k_{ij} I_0 (\gamma \, \mathrm{e}^{-\alpha x} + (1-\gamma) \, \mathrm{e}^{-\alpha(1-x)}) c_i \tag{2}$$

This case is illustrated by Figs. 1–3, where $\gamma = 1$.

The system of dimensionless conservation equations describing flow and reaction in the photocatalyst layer is:

$$\frac{\mathrm{d}\mathbf{y}}{\mathrm{d}x} + \mathbf{K}(\gamma \, \mathrm{e}^{-\alpha x} + (1-\gamma) \, \mathrm{e}^{-\alpha(1-x)})\mathbf{y} = 0, \quad \mathbf{y}(0) = \mathbf{y}_0 \tag{3}$$

where $\mathbf{y}$ is the vector of real-species mole fractions, $y_i = c_i/c_0$, and where c_0 can be chosen as either the total molar concentration of the solution or the total molar concentration of only the reacting species. $\mathbf{K}$ is the dimensionless rate coefficient matrix, which is formed by the rate coefficients each multiplied by the total incident light intensity and by the superficial residence time of water in the layer, τ. For a system with three species:

$$\mathbf{K} = I_0 \tau \begin{bmatrix} (k_{AB} + k_{AC}) & -k_{BA} & -k_{CA} \\ -k_{AB} & (k_{BA} + k_{BC}) & -k_{CB} \\ -k_{AC} & -k_{BC} & (k_{CA} + k_{CB}) \end{bmatrix} \tag{4}$$

$$\tau = \frac{AL}{Q} \tag{5}$$

where A is the geometric area of the layer face, L is the thickness of the layer, and Q is the volumetric flow rate of water through the layer. Dispersion of species in the direction of flow was found to be significant in air purification applications [23]. Although dispersion can be accommodated by the method [20], it was assumed negligible because diffusion coefficients in water are much smaller than in air, whereas other values which characterize the ratio of convective to diffusive transport are similar in air and water applications. Below, lowercase bold letters are column vectors and uppercase bold letters are matrices.

The eigenvector matrix $\mathbf{X}$ and diagonal eigenvalue matrix $\mathbf{\Lambda}$ of $\mathbf{K}$ are given by:

$$\mathbf{K}\mathbf{X} = \mathbf{X}\mathbf{\Lambda} \tag{6}$$

The inverse of $\mathbf{X}$ transforms the real-species into the so-called characteristic species [18] or eigenspecies [22] whose individual concentrations are z_i, which are elements of vector $\mathbf{z}$:

$$\mathbf{X}^{-1}\mathbf{y} = \mathbf{z} \tag{7}$$

Since $\mathbf{\Lambda}$ is diagonal, the eigenspecies flow and react independently of each other:

$$\frac{\mathrm{d}\mathbf{z}}{\mathrm{d}x} + \mathbf{\Lambda}(\gamma \, \mathrm{e}^{-\alpha x} + (1-\gamma) \, \mathrm{e}^{-\alpha(1-x)})\mathbf{z} = 0, \quad \mathbf{z}(0) = \mathbf{z}_0 \tag{8}$$

The solution for each of n species is:

$$z_i = z_{i,0} \frac{\exp((\lambda_i/\alpha)(\gamma \, \mathrm{e}^{-\alpha x} - (1-\gamma) \, \mathrm{e}^{-\alpha(1-x)}))}{\exp((\lambda_i/\alpha)(\gamma - (1-\gamma) \, \mathrm{e}^{-\alpha}))} = z_{i,0}\omega_i, \quad i = 1, 2, \ldots, n \tag{9}$$

where the λ_i are the diagonal elements of $\mathbf{\Lambda}$. As α approaches zero, the solution approaches that for reaction in a plug-flow reactor in the absence of illumination or at constant illumination. The solution for an eigenspecies also applies to a single real-species reacting irreversibly to a single product species, where $z = c$ and $\lambda = kI_0\tau$.

At $x = 1$, $\mathbf{z}$ and, thus, $\mathbf{y}$ are invariant with γ. That is, for constant total illumination intensity, the outlet composition is invariant with changes in the distribution of the intensity

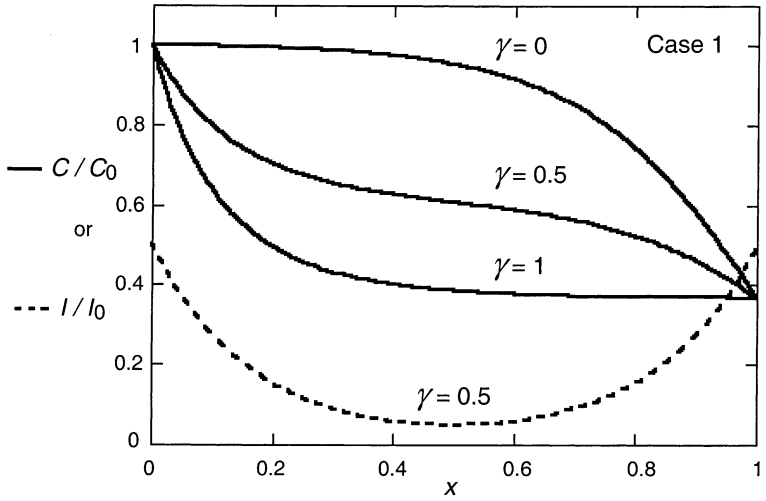

Fig. 4. Reactant concentration profiles across a photocatalyst layer through which water flows (case 1) for the parameter values $\lambda = \alpha = 6$. The direction of water flow is from left to right with increasing dimensionless position x. Concentration curves for three different values of γ are shown, where γ is the fraction of total illumination intensity impinging on the water inlet face of the layer and where the total illumination intensity is constant for all three cases. The outlet concentration is invariant with γ. The lower curve is the local light intensity for the case of $\gamma = 0.5$. For the other two cases, the local intensity falls off exponentially, from a value of 1 to a value of almost 0, from left to right for $\gamma = 1$ and from right to left for $\gamma = 0$.

between the inlet and outlet faces. Fig. 4 shows concentration profiles across a photocatalyst layer which illustrate this invariance with light distribution. The dimensionless concentrations shown are that of a single eigenspecies, or of a single real-species that reacts irreversibly to a single product species. In the later case, values of τ, α, and I_0 can be used with the measured concentration change across the layer and Eq. (9) to determine the value of the single intrinsic rate coefficient k.

For a system with three species

$$\mathbf{z} = \begin{bmatrix} \omega_1 & 0 & 0 \\ 0 & \omega_2 & 0 \\ 0 & 0 & \omega_3 \end{bmatrix} \mathbf{z}_0 = \mathbf{\Omega z}_0 \tag{10}$$

The reverse-transformation gives the mole fractions of the real-species at location x in the photocatalyst layer:

$$\mathbf{y} = \mathbf{X\Omega X}^{-1}\mathbf{y}_0 \tag{11}$$

Thus, with known rate coefficients and other system parameters, outlet mole fractions can be obtained given inlet mole fractions. Usually, however, the first objective will be to determine rate coefficients values from experimental measurements. The method of Herz and Hegedus [22] is used to analyze the points in Fig. 2.

For the points in Fig. 2, the composition at the photocatalyst inlet $\mathbf{y}_0$ is equal to the composition measured in the reservoir. The composition at the photocatalyst outlet $\mathbf{y}_1$ at each time t is determined from material balances:

$$y_{i1} = y_{i0} + \left(\frac{V}{Q}\right)\frac{\mathrm{d}y_{i0}}{\mathrm{d}t}, \quad i = 1, 2, \ldots, n \tag{12}$$

To analyze the points in Fig. 2 and obtain the derivatives $\mathrm{d}y_{i0}/\mathrm{d}t$, groups of five points were formed by selecting the first five points in the time series to make the first group, then dropping the first point and adding the sixth point in the series to form the second group, and so forth, producing m groups from $(m + 4)$ points. The choice of number of points per group in numerical differentiation is dependent on signal-to-noise level and other factors. Each group of five points was fit to a quadratic polynomial and the slope $\mathrm{d}y_{i0}/\mathrm{d}t$ of the polynomial was evaluated at the mid-point time in the group. The m pairs of composition vectors that result from using this numerical differentiation procedure and Eq. (12) form the $n \times m$ matrices $\mathbf{Y}_1$ and $\mathbf{Y}_0$:

$$\begin{bmatrix} \mathbf{y}_{11} & \mathbf{y}_{12} & \cdots & \mathbf{y}_{1m} \end{bmatrix} = \mathbf{X\Omega X}^{-1} \begin{bmatrix} \mathbf{y}_{01} & \mathbf{y}_{02} & \cdots & \mathbf{y}_{0m} \end{bmatrix} \tag{13}$$

$$\mathbf{Y}_1 = \mathbf{X\Omega X}^{-1}\mathbf{Y}_0 \tag{14}$$

When the number of pairs of composition vectors equals the number of species, the $n \times m = n \times n$ matrix $\mathbf{Y}_0$ can be inverted to obtain:

$$[\mathbf{Y}_1\mathbf{Y}_0^{-1}]\mathbf{X}_{\mathrm{expl}} = \mathbf{X}_{\mathrm{expl}}\mathbf{\Omega}_{\mathrm{expl}}, \quad m = n \tag{15}$$

The eigenvector matrix $\mathbf{X}_{\mathrm{expl}}$ is an estimate of the eigenvector matrix $\mathbf{X}$ of the original rate coefficient matrix, and the eigenvalue matrix $\mathbf{\Omega}_{\mathrm{expl}}$ contains estimates of the eigenvalues. In order to get better estimates of rate coefficients, a greater number of measurements should be made, resulting in an over-determined system. Multiplying both sides from the right by $\mathbf{Y}_0^{\mathrm{T}}$ gives:

$$[\mathbf{Y}_1\mathbf{Y}_0^{\mathrm{T}}] = [\mathbf{X\Omega X}^{-1}]_{\mathrm{expl}}[\mathbf{Y}_0\mathbf{Y}_0^{\mathrm{T}}], \quad m > n \tag{16}$$

which is the set of normal equations [24] for the least-squares approximation of $[\mathbf{X\Omega X}^{-1}]_{\mathrm{expl}}$. The $n \times n$ matrix $[\mathbf{Y}_0\mathbf{Y}_0^{\mathrm{T}}]$ can be inverted, thus, $\mathbf{X}_{\mathrm{expl}}$ and $\mathbf{\Omega}_{\mathrm{expl}}$ can be determined by

solving the eigenvalue problem:

$$[[\mathbf{Y}_1\mathbf{Y}_0^{\mathrm{T}}][\mathbf{Y}_0\mathbf{Y}_0^{\mathrm{T}}]^{-1}]\mathbf{X}_{\mathrm{expl}} = \mathbf{X}_{\mathrm{expl}}\boldsymbol{\Omega}_{\mathrm{expl}}, \quad m > n \tag{17}$$

Finally, with α determined in separate measurements, $\boldsymbol{\Lambda}_{\mathrm{expl}}$ can be determined from $\boldsymbol{\Omega}_{\mathrm{expl}}$ and the estimate of the rate coefficient matrix obtained:

$$\lambda_i = \frac{\alpha(-\ln \omega_i)}{1 - \mathrm{e}^{-\alpha}}, \quad x = 1,\ \gamma = 1 \tag{18}$$

$$\mathbf{K}_{\mathrm{expl}} = \mathbf{X}_{\mathrm{expl}}\boldsymbol{\Lambda}\mathbf{X}_{\mathrm{expl}}^{-1} \tag{19}$$

Eigenvalues and eigenvectors can be obtained conveniently using mathematical software such as MATLAB [25] and Mathematica [26]. Since the eigenvalue of the eigenspecies that corresponds to the equilibrium composition of the real-species mixture has a value of zero, zeroing the smallest λ_i estimate improves estimates of $\mathbf{K}$. For a given system, estimated values will vary with degree of error, number of composition measurements, and specific values obtained by the measurements. For the same input values, number of data points, and level of simulated error, repeating the data point generation and analysis in this example gives rate coefficient estimates within ±10% of the input values. At relatively high error level and low number of measurements, the eigenvalues and vectors may not be obtainable, and iterative optimization of the real-species model would be required to estimate intrinsic rate coefficients.

Table 1 compares the input rate coefficients in $\mathbf{K}$ with those in $\mathbf{K}_{\mathrm{expl}}$ determined by analysis of the points in Fig. 2. The curves in Fig. 2 were generated from $\mathbf{K}_{\mathrm{expl}}$ and show that reasonable estimates were obtained. If one were to ignore the light and concentration gradients in the photocatalyst layer, analysis of the initial rate of decay of species A in Fig. 2 gives an apparent $k'_{\mathrm{AB}} = 0.36\,\mathrm{s}^{-1}$, substantially less than the true value of $1.0\,\mathrm{s}^{-1}$.

3. Case 2—diffusion into layer, light on external face

In cases 2 and 3, the external face of the photocatalyst layer is exposed to a well-mixed cell through which water flows. The other face of the layer is sealed or otherwise impermeable, except in the case of mineralization of contaminants, where this face may be permeable to CO_2. Species diffuse into the layer and react.

Fig. 5 shows concentration profiles of a reactant within a photocatalyst layer for light incident on the external face exposed to flowing water (case 2) and light incident on the sealed face of the layer (case 3), as computed with the solutions obtained below for example conditions.

As Chen et al. [17] demonstrated, external mass transfer resistance in the fluid boundary layer over the photocatalyst can affect reaction rates. This external resistance can be made negligible by stirring or pumping water at sufficiently high rates over the layer such that the composition in the bulk water approaches the composition at the water–catalyst interface. The solutions obtained here for composition within a photocatalyst layer apply regardless of the significance of external transport resistance. The presence of significant external resistance does have to be considered when calculating overall reaction rates. External transport resistance is specified to have made negligible here in order to simplify the equations and explanations below, although external resistance can be incorporated into the solution of this linear system without difficulty when desired.

The system of equations describing the real-species is:

$$\frac{\mathrm{d}^2\mathbf{y}}{\mathrm{d}x^2} - [\phi^2]\,\mathrm{e}^{-\alpha x}\mathbf{y} = 0, \quad \mathbf{y}(0) = \mathbf{y}_0, \quad \left.\frac{\mathrm{d}\mathbf{y}}{\mathrm{d}x}\right|_{x=1} = 0 \tag{20}$$

$$[\phi^2] = L^2 I_0 \mathbf{K}\mathbf{D}^{-1} \tag{21}$$

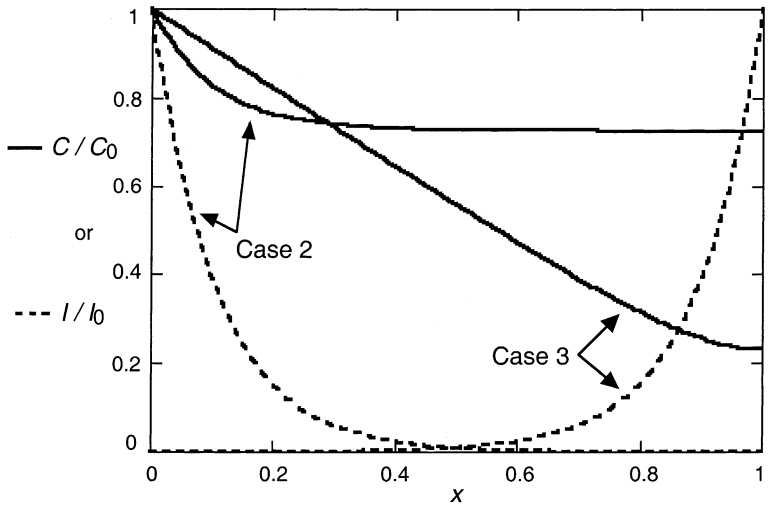

Fig. 5. Reactant concentration and light intensity profiles within a catalyst layer into which reactants penetrate by diffusion (cases 2 and 3). The conditions shown here are the conditions at $L = 15\,\mu\mathrm{m}$ in Fig. 6: $\lambda = 5.5$, $\alpha = 9.4$. The external face exposed to flowing water is on the left ($x = 0$) and the sealed face of the layer is on the right ($x = 1$).

where **D** is the diagonal matrix of effective diffusion coefficients of species in the layer. To simplify notation below, we consider a case in which the effective diffusion coefficients D_{eff} are equal:

$$[\phi^2] = \frac{L^2 I_0}{D_{\text{eff}}}\mathbf{K} \tag{22}$$

The eigenvector matrix **X** and diagonal eigenvalue matrix $[\lambda^2]$ of the non-diagonal matrix $[\phi^2]$ are given by:

$$[\phi^2]\mathbf{X} = \mathbf{X}[\lambda^2] \tag{23}$$

The system of equations describing diffusion and reaction of the eigenspecies is:

$$\frac{\mathrm{d}^2\mathbf{z}}{\mathrm{d}x^2} - [\lambda^2]\,\mathrm{e}^{-\alpha x}\mathbf{z} = 0, \quad \mathbf{z}(0) = \mathbf{z}_0, \qquad \left.\frac{\mathrm{d}\mathbf{z}}{\mathrm{d}x}\right|_{x=1} = 0 \tag{24}$$

The Thiele modulus [16], at constant light intensity, of eigenspecies i is λ_i. Solutions are given for equimolar counter diffusion and apply for the dilute solutions considered:

$$z_i = z_{i0}\frac{K_1(-f_{i1})I_0(f_{i2}(x)) - K_0(-f_{i2}(x))I_1(f_{i1})}{K_1(-f_{i1})I_0(f_{i3}) - K_0(-f_{i3})I_1(f_{i1})}, \quad i = 1, 2, \ldots, n \tag{25}$$

where $K_{0/1}$ and $I_{0/1}$ are modified (hyperbolic) Bessel functions [27], and where

$$f_{i1} = 2\left(\frac{\lambda_i}{\alpha}\right)\mathrm{e}^{-\alpha/2}, \qquad f_{i2}(x) = 2\left(\frac{\lambda_i}{\alpha}\right)\mathrm{e}^{-\alpha x/2},$$
$$f_{i3} = 2\left(\frac{\lambda_i}{\alpha}\right) \tag{26}$$

The solution for an eigenspecies also applies to a single real-species reacting irreversibly to a single product species, where $z = c$ and $\lambda^2 = kI_0L^2/D_{\text{eff}}$.

The internal effectiveness factor η_i for each eigenspecies is a measure of the extent to which diffusion resistance and light absorption reduce the reaction rate. The effectiveness factor is equal to the actual rate of reaction in the photocatalytic layer divided by the rate that would be obtained if all active sites in the layer were exposed to the incident illumination intensity and the water composition at the external face. The actual rate of reaction in the photocatalytic layer is equal to the rate at which reactant diffuses into the layer at the external face:

$$\eta_i = \frac{1}{\lambda_i^2}\left(-\left.\frac{\mathrm{d}z_i}{\mathrm{d}x}\right|_{x=0}\right) \tag{27}$$

$$\eta_i = \left(\frac{1}{\lambda_i}\right)\frac{K_1(-f_{i1})I_1(f_{i3}) - K_1(-f_{i3})I_1(f_{i1})}{K_1(-f_{i1})I_0(f_{i3}) - K_0(-f_{i3})I_1(f_{i1})} \tag{28}$$

As α approaches zero, the solutions for the photocatalytic diffusion cases approach the solutions for reaction in the absence of illumination or at constant illumination [16]:

$$\lim_{\alpha\to 0} z_i = z_{i0}\frac{\mathrm{e}^{\lambda_i x} + \mathrm{e}^{-\lambda_i x}}{\mathrm{e}^{\lambda_i} + \mathrm{e}^{-\lambda_i}} = z_{i0}\frac{\cosh(\lambda_i x)}{\cosh(\lambda_i)} \tag{29}$$

$$\lim_{\alpha\to 0}\eta_i = \left(\frac{1}{\lambda_i}\right)\frac{\mathrm{e}^{\lambda_i} - \mathrm{e}^{-\lambda_i}}{\mathrm{e}^{\lambda_i} + \mathrm{e}^{-\lambda_i}} = \frac{\tanh(\lambda_i)}{\lambda_i} \tag{30}$$

The method for estimating rate coefficients differs somewhat from case 1. Here, a balance on an eigenspecies gives:

$$Q(z_i^{\text{in}} - z_{i0}) = -AD_{\text{eff}}\left.\frac{\mathrm{d}z_i}{\mathrm{d}x}\right|_{x=0} \tag{31}$$

where z_i^{in} is the concentration of eigenspecies i in the reservoir and at the inlet to the well-mixed reaction cell enclosing the photocatalyst, and z_{i0} is the concentration in the reaction cell over the external face of the photocatalyst:

$$z_i^{\text{in}} = \left[1 - \frac{AD_{\text{eff}}}{Q}\left(\frac{1}{z_{i0}}\left.\frac{\mathrm{d}z_i}{\mathrm{d}x}\right|_{x=0}\right)\right]z_{i0} \tag{32}$$

$$z_i^{\text{in}} = \left[1 + \left(\frac{AD_{\text{eff}}}{Q}\right)\eta_i\lambda_i^2\right]z_{i0} = \omega_i z_{i0} \tag{33}$$

$$\mathbf{z}^{\text{in}} = \mathbf{\Omega}\mathbf{z}_0 \tag{34}$$

$$\mathbf{y}^{\text{in}} = \mathbf{X}\mathbf{\Omega}\mathbf{X}^{-1}\mathbf{y}_0 \tag{35}$$

where the ω_i are the diagonal elements of the diagonal matrix **Ω**. Consider a system similar to that shown in Fig. 1 but with water flow over one face of the photocatalyst layer rather than through the layer. The mole fractions in the reaction cell, y_{i0}, are determined from material balances:

$$y_{i0} = y_i^{\text{in}} + \left(\frac{V}{Q}\right)\frac{\mathrm{d}y_i^{\text{in}}}{\mathrm{d}t} \tag{36}$$

where y_i^{in} are mole fractions of the real-species in the reservoir and at the inlet to the reaction cell. A set of m experimental measurements form the matrices $\mathbf{Y}^{\text{in}}$ and $\mathbf{Y}_0$:

$$\mathbf{Y}^{\text{in}} = \mathbf{X}_{\text{expl}}\mathbf{\Omega}_{\text{expl}}\mathbf{X}_{\text{expl}}^{-1}\mathbf{Y}_0 \tag{37}$$

where $\mathbf{\Omega}_{\text{expl}}$ is the diagonal matrix of the ω_i. As in case 1, the experimental measurements allow estimation of the eigenvector matrix $\mathbf{X}_{\text{expl}}$ and the eigenvalue matrix $\mathbf{\Omega}_{\text{expl}}$:

$$[[\mathbf{Y}^{\text{in}}\mathbf{Y}_0^{\text{T}}][\mathbf{Y}_0\mathbf{Y}_0^{\text{T}}]^{-1}]\mathbf{X}_{\text{expl}} = \mathbf{X}_{\text{expl}}\mathbf{\Omega}_{\text{expl}}, \quad m > n \tag{38}$$

With measurements or estimates of A, D_{eff}, Q, and α, a root-finding algorithm can be used to determine the λ_i from the ω_i in order to form $[\lambda^2]$. Finally, the rate coefficient matrix can be obtained from:

$$[\phi^2]_{\text{expl}} = \mathbf{X}_{\text{expl}}[\lambda^2]_{\text{expl}}\mathbf{X}_{\text{expl}}^{-1} \tag{39}$$

$$\mathbf{K}_{\text{expl}} = \left(\frac{D_{\text{eff}}}{L^2 I_0}\right)[\phi^2]_{\text{expl}} \tag{40}$$

4. Case 3—diffusion into layer, light on impermeable face

For this case, the direction of the spatial coordinate x has been reversed such that x=0 is at the impermeable face of the layer. The governing equations are the same as the first diffu-

sion case except that the boundary conditions have changed:

$$\frac{d^2\mathbf{z}}{dx^2} - [\lambda^2]\,e^{-\alpha x}\mathbf{z} = 0,$$
$$\left.\frac{d\mathbf{z}}{dx}\right|_{x=0} = 0, \quad \mathbf{z}(1) = \mathbf{z}_1 = \mathbf{X}^{-1}\mathbf{y}_1 \tag{41}$$

The solution is:

$$z_i = z_{i1}\frac{K_0(-f_{i2}(x))I_1(f_{i3}) - K_1(-f_{i3})I_0(f_{i2}(x))}{K_0(-f_{i1})I_1(f_{i3}) - K_1(-f_{i3})I_0(f_{i1})}, \quad i = 1, 2, \ldots, n \tag{42}$$

The effectiveness factors are:

$$\eta_i = \left(\frac{e^{-\alpha/2}}{\lambda_i}\right)\frac{K_1(-f_{i3})I_1(f_{i1}) - K_1(-f_{i1})I_1(f_{i3})}{K_0(-f_{i1})I_1(f_{i3}) - K_1(-f_{i3})I_0(f_{i1})} \tag{43}$$

5. Comparison of cases

For a single eigenspecies, or a system with only two real species, the fractional conversion of reactant across the reaction cell, δ, for the flow-through case (case 1) with light incident on the inlet face is greater than for the diffusion case with light incident on the external face (case 2):

$$\frac{\delta_i^{\text{flow}}}{\delta_i^{\text{diff}}} = \frac{1-\omega_i^{\text{flow}}}{\lambda_i^{\text{flow}}\eta_i^{\text{diff}}/(1+\lambda_i^{\text{flow}}\eta_i^{\text{diff}})} > 1$$
$$\text{in } \eta_i^{\text{diff}}, \lambda_i^{\text{diff}} = \left(\frac{\lambda_i^{\text{flow}}L^2/D_{\text{eff}}}{AL/Q}\right)^{0.5} \tag{44}$$

where ω_i^{flow} and η_i^{diff} are functions given above by Eqs. (9) and (28), respectively, and where all conditions except the flow configuration are the same for both cases. Although conversions are lower for the diffusion case, it may be preferred for water ultrapurification where CO_2 is removed across the internal face of a photocatalytic membrane, or for other reasons.

The ratios of effectiveness factors for cases 2 and 3 are:

$$\frac{\eta_i^{\text{case 2}}}{\eta_i^{\text{case 3}}} = e^{\alpha/2}\frac{K_1(-f_{i3})I_0(f_{i1}) - K_0(-f_{i1})I_1(f_{i3})}{K_1(-f_{i1})I_0(f_{i3}) - K_0(-f_{i3})I_1(f_{i1})} > 1 \quad \text{for all } \lambda_i, \alpha > 0 \tag{45}$$

That is, higher average reaction rates will be obtained for illumination on the external face than will be obtained for illumination on the impermeable face of a layer in which reactants diffuse. This result is demonstrated in Fig. 5, where all conditions are the same for the two cases except for the direction of illumination, and where concentration profiles are shown for a single eigenspecies or a single real reactant species that reacts irreversibly to a single product. The lower rate obtained for light illuminating the sealed face (light from right side of figure) can be seen by the lower concentration gradient at the water–catalyst interface at $x = 0$, where the same direction of x has been used for both cases in the figure.

For a single reactant species reacting irreversibly to a single product in a layer of thickness L, the overall rate per unit area of catalyst layer is:

$$r\,(\text{mol s}^{-1}\,\text{m}^{-2}) = kI_0c_0L\eta \tag{46}$$

where c_0 is the reactant concentration at the external, water–catalyst interface. For a single eigenspecies or a single real-species reacting irreversibly to a single product, Fig. 6 plots curves of relative rate $r/r_{\max}$ versus layer thickness L for the two diffusion cases, where:

$$\frac{r}{r_{\max}} = \frac{\lambda\eta}{(\lambda\eta)_{\max,\,\text{case 2}}} \tag{47}$$

Fig. 6 shows that, for illumination of the external water–catalyst interface (case 2), the overall rate approaches

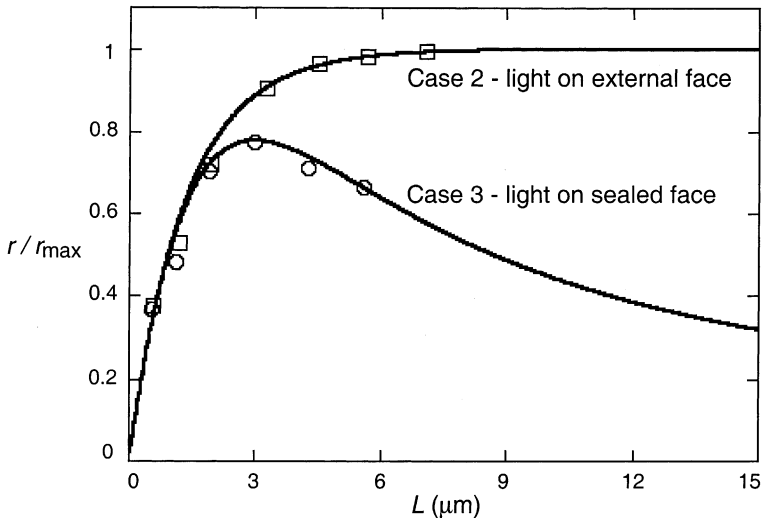

Fig. 6. The dependence of overall reaction rate on photocatalyst layer thickness for the two diffusion cases (cases 2 and 3). The data points are from Figs. 8 and 9 of Ref. [17]. The curves were computed from the solutions obtained here using values of L, D_{eff}, and α' (m^{-1}) determined in Ref. [17] and by adjusting the value of kI_0 to fit the curves to the points. This results in an estimate of the intrinsic reaction rate coefficient for the system of Ref. [17].

a limiting value as layer thickness increases because the addition of relatively dark catalyst near the sealed interface does not add to the rate or affect diffusion resistance ahead of the reaction zone. In contrast, for illumination of the sealed face (case 3), Fig. 6 shows that the overall rate goes through a maximum with increasing layer thickness. Chen et al. [17] reached the same conclusions in their analysis of configurations equivalent to cases 2 and 3, although they assumed that the concentration profiles were simple exponentials in their derivations. Fig. 5 shows the actual concentration profiles for the two cases at $L = 15\,\mu$m in Fig. 6 which, along with Eqs. (25) and (42) above, demonstrate that the profiles are not simple exponentials. For case 3, the rate decreases as layer thickness increases past the rate maximum because the relatively dark and inactive portion of the layer near the water–catalyst interface adds increasing diffusion resistance ahead of the reaction zone near the sealed and illuminated surface. The left side of the concentration profile for case 3 in Fig. 5 approaches the linear shape of diffusion through an inactive zone.

Experimental data of Chen et al. [17] for the reaction of benzoic acid in water over TiO_2 can be analyzed, using the results obtained here, to obtain an estimate of the intrinsic rate coefficient. TiO_2 layers in [17] were illuminated with incident light intensity of $213\,W/m^2$ with a sharp primary peak at a wavelength of 365 nm. The points in Fig. 6 are experimental data from Figs. 8 and 9 of Ref. [17]. The values of L, D_{eff}, and α' (m^{-1}) determined in Ref. [17] were used in computing the curves in Fig. 6. Since the data for the case 3 configuration were normalized separately from the data for case 2 in [17], the case 3 data points were adjusted so that the maximum data point value matched the case 3 curve maximum in Fig. 6. The value of the intrinsic reaction rate coefficient, $k' = kI_0$, was varied in order to fit the curves to the data points. The value determined was $k' = 13\,s^{-1}$.

6. Conclusions

Analytical solutions can be obtained for arbitrary networks of first-order reactions in photocatalytic layers for several flow and illumination geometries. These solutions demonstrate the significant influence of concentration and light intensity gradients in the layers on measured reaction rates. The solutions can be used to analyze experimental data in order to extract intrinsic rate coefficients. Reactions with nonlinear kinetics will require different solution procedures but internal gradients will be important in these systems as well.

Acknowledgements

This work was supported by the US National Science Foundation grant DUE-0125076 and by the NSF/SRC Engineering Research Center for Environmentally Benign Semiconductor Manufacturing at the University of Arizona. Discussions with F. Shadman and R. Morris at the University of Arizona are appreciated.

References

[1] M. Anpo, H. Yamashita, in: M. Schiavello (Ed.), Heterogeneous Photocatalysis, Wiley, New York, 1997, p. 133.
[2] I.-R. Subbotina, B.-N. Shelimov, V.-B. Kazansky, J. Catal. 184 (1999) 390.
[3] K. Domen, M. Hara, J.N. Kondo, T. Takata, A. Kudo, H. Kobayashi, Y. Inoue, Korean J. Chem. Eng. 18 (2001) 862.
[4] D.F. Ollis, Comptes Rendus Acad. Sci. Ser. II C 3 (2000) 405.
[5] J.M. Herrmann, in: F.J.J. Janssen, R.A. VanSanten (Eds.), Environmental Catalysis, Imperial College Press, London 1999, p. 171.
[6] P. Pichat, J. Disdier, C. Hoang-Van, D. Mas, G. Goutailler, C. Gaysse, Catal. Today 63 (2000) 363.
[7] R. Molinari, L. Palmisano, E. Drioli, M. Schiavello, J. Membr. Sci. 206 (2002) 399.
[8] R. Molinari, M. Mungari, E. Drioli, A. Di Paola, V. Loddo, L. Palmisano, M. Schiavello, Catal. Today 55 (2000) 71.
[9] A. Fernandez, G. Lassaletta, V.M. Jimenez, A. Justo, A.R. Gonzalez-Elipe, J.M. Herrmann, H. Tahiri, Y. Ait-Ichou, Appl. Catal. B 7 (1995) 49.
[10] R.W. Matthews, Solar Energy 38 (1987) 405.
[11] K.T. Kin, F. Shadman, IEEE Transactions on Semiconductor Manufacturing 13 (2000) 1.
[12] O. Borio, B.M. Gawlik, I.R. Bellobono, H. Muntau, Chemosphere 37 (1998) 975.
[13] L. Rivas, I.R. Bellobono, F. Ascari, Chemosphere 37 (1998) 1033.
[14] L. Tatti, D. Niego, F. Rota, P. Burzzi, A. Moroni, I.R. Bellobono, Chemosphere 34 (1997) 41.
[15] D.F. Ollis, Environ. Sci. Technol. 19 (1985) 480.
[16] O. Levenspiel, Chemical Reaction Engineering, 3rd ed., Wiley, New York, 1999.
[17] D. Chen, F. Li, A.K. Ray, Catal. Today 66 (2001) 475.
[18] J. Wei, C.D. Prater, Adv. Catal. 13 (1962) 203.
[19] J. Wei, J. Catal. 1 (1962) 526.
[20] T.B. Clement, Water Resour. Res. 37 (2001) 157.
[21] G.R. Gavalas, AIChE J. 19 (1973) 214.
[22] R.K. Herz, L.L. Hegedus, Chem. Eng. Sci. 33 (1978) 1561.
[23] D.F. Ollis, Ind. Eng. Chem. Res. 41 (2002) 6409.
[24] R.L. Burden, J.D. Faires, Numerical Analysis, 7th ed., Brooks/Cole-Thomson Learning, Pacific Grove, CA, 2001.
[25] MATLAB(TM), The MathWorks, Inc., Natick, MA.
[26] Mathematica(TM), Wolfram Research, Inc., Champaign, IL.
[27] D. Zwillinger (Ed.), CRC Standard Mathematical Tables and Formulae, 30th ed., CRC Press, Boca Raton, FL, 1996.